Praise Worthy Prize

This paper is available online at www.praiseworthyprize.org
International Review on Modelling and Simulations (I.RE.MO.S.), Vol. 16, N. 3
ISSN 1974-9821 *June 2023*

Investigating the Impact of Temperature and Interlayer Defects on the Efficiency of Mo/ZnTe/ZnSe/SnO_2 Heterojunction Thin Film Solar Cells: a SCAPS-1D Simulation Study

Samer H. Zyoud[1, 2], Ahed H. Zyoud[3]

Abstract – *This study investigates the effect of using SnO_2 as a window layer in a heterojunction Mo/ZnTe/ZnSe/SnO_2 thin film-solar cell, which, when compared to other absorber layer materials, has the potential to be used in solar photovoltaic applications due to its low cost, non-toxic nature, and ease of availability. The research has aimed to compare the impact of SnO_2 with ZnO, which has been previously used as a window layer. Numerical modeling using the Solar Cell Capacitance Simulator (SCAPS-1D) has been conducted to analyze the effect of temperature and defects in the thin-film layers on the overall performance of the solar cell. Efficiency parameters such as short-circuit current density J_{SC}, open-circuit voltage V_{OC}, fill factor FF, and efficiency η, have been found to be influenced by temperature, and the effect of defects between the layers was analyzed. The optimal operating temperature for the solar cell with SnO_2 as a window layer has been found to be 375 K, which has not required cooling to maintain cell efficiency, unlike the optimal operating temperature of 300 K for the solar cell with ZnO as a window layer. The simulation results have showed that using SnO_2 as a window layer is advantageous due to the higher optimal operating temperature and the absence of the need for cooling to maintain cell efficiency. The study highlights the significance of quality control during fabrication in order to minimize defects and enhance the efficiency of the solar cell.* ***Copyright © 2023 The Authors.***

Keywords: *Thin Film Solar Cell, Mo/ZnTe/ZnSe/SnO_2, SCAPS-1D, Photovoltaic*

Nomenclature

A	Area
B	Independently temperature constant
CB	Conductance Band
D	Diffusivity of the minority carrier
e	Elementary charge (1.6×10^{-19} C)
E_C	Conduction band potential
E_F	Fermi level energy
E_G	Bandgap
E_{G0}	Extrapolated bandgap at 0 K
E_V	Valance band potential
E_t	Total defect energy
EFn	Quasi Fermi level for electrons
EFp	Quasi Fermi level for holes
Ei	Intrinsic level
FF	Fill Factor
G	Generation rate
h	Blank constant
I_o	Maximum current
I_S	Saturation current
I_{SC}	Short-circuit current
J_n	Electron current densities
J_p	Hole current densities
J_{SC}	Short-circuit current density
k	Constant
L	Diffusion length of the minority carrier
MO	Molybdenum
m_e^*	Effective electron mass
m_h^*	Effective hole mass
n	Electrons concentration
N_A	Charged impurities of acceptor
N_C	CB effective density of states
N_D	Charged impurities of donor
N_V	VB effective density of states
p	Holes concentration
PV	Photovoltaic
q	Electron charge
QE%	Quantum Efficiency percent
R	Recombination rate
SCAPS-1D	Solar Cell Capacitance Simulator in 1 Dimension
SnO_2	Tin(IV) oxide
n_i	Intrinsic carrier concentration
T	Temperature
VB	Valance Band
V_{OC}	Open-Circuit voltage
$V_{e\text{-}th}$	Electron thermal velocity
$V_{p\text{-}th}$	Hole thermal velocity
W	Thickness

Available online by June 30th, 2023 https://doi.org/10.15866/iremos.v16i3.22739

ZnSe	Zinc selenide
ZnTe	Zinc Telluride
η	Efficiency
λ	Wavelength
Ψ	Electrostatic potential
ϵ_o	Vacuum permittivity
ϵ_r	Relative permittivity
ε_r	Dielectric permittivity (relative)
μ_e	Electron mobility
μ_p	Hole mobility
ρ_p	Holes distribution
ρ_n	Electrons distribution
χ_e	Electron affinity

I. Introduction

The use of numerical modeling has been widely employed in the optimization of various processes, including energy [1], [2], transportation [3]-[5], production planning [6], [7], water and food production [8], [9] and others fields [10], [11]. In the field of solar energy, numerical simulation has been used to improve the properties of solar cells [12]-[14]. One type of emerging solar cell is the nanostructured thin film of metal oxides, which has attracted increased interest for its simplicity and ease of manipulation [15], [16]. Zinc telluride (ZnTe) is a promising candidate for the development of low-cost and high-efficiency thin film solar cells due to its ability to create a p-n junction with an n-type CdS thin layer that is advantageous for photovoltaic solar energy conversion. However, ZnTe's high band gap limits its ability to absorb photons in the visible spectrum, which reduces conversion efficiency. Most II-VI semiconductor-based solar cells use CdTe thin films as absorbers, with thicknesses and conversion efficiencies of 16-25% [17]. A numerical study has been conducted to determine the influence of ZnTe thickness on solar cell performance, and the maximum efficiency has been found to be 10% at the optimum thickness of approximately 2 μm [18]. Temperature also plays a significant role in the performance of solar cells, and simulations have been used to study the effect of operating temperature on solar panel efficiency [19]-[22]. Operating temperature is one of the most important factors in the performance of solar cells, affecting efficiency parameters such as V_{OC}, J_{SC}, *FF*%, η%, and *QE*% [21], [23]. Due to faster electron and hole recombination, an increase in operating temperature typically results in a decrease in V_{OC} and an increase in reverse saturation current. The efficiency of solar cells also decreases as the temperature increases due to the reduction of the band-gap of most semiconductor materials and the negative effect on electron and hole mobility, carrier concentrations, and bandgaps of the material [19], [20], [23]-[25]. The open-circuit voltage originally decreases with increasing temperature because of the temperature dependence of the I_o:

$$I_o = qA\frac{Dn_i^2}{LN_D} \tag{1}$$

Among the above parameters, the intrinsic carrier concentration (n_i) is the most significantly impacted by temperature, where *D* represents the diffusivity of the minority carrier, *L* represents the diffusion length of the minority carrier, and N_D represents doping:

$$n_i^2 = 4\left(\frac{2\pi kT}{h^2}\right)^3 (m_e^* m_h^*)^{3/2} e^{-\frac{E_{G0}}{kT}} = BT^3 e^{-\frac{E_{G0}}{kT}} \tag{2}$$

The equation for the open-circuit voltage (V_{OC}) can be obtained by substituting the equation for the intrinsic carrier concentration (n_i) into the equation for I_o. This equation includes the variables *T* (temperature), *B* (independently temperature constant), E_{G0} (extrapolated bandgap at absolute zero), and *k* (constant). The equation is given by:

$$V_{OC} = \frac{kT}{q}\ln\frac{I_{SC}}{I_O} \tag{3}$$

where *q* is the elementary charge. The impact of temperature on V_{OC} is reflected in the temperature-dependent variables in the equation.

The SCAPS-1D program is a simulation tool developed by a research group at the University of Gent [23], [24], [26]-[28] and utilizes equations from literature for the numerical calculation of thin-film solar cell devices [27].

The purpose of this study is to investigate the effects of temperature and interlayer defects on the performance of a Mo/ZnTe/ZnSe/SnO_2 heterojunction solar cell, by using the SCAPS-1D program. Previous research on ZnTe/ZnSe/ZnO thin-film photovoltaic solar cells has shown that in order to achieve optimal performance, the device should be maintained at a temperature of 300K, which requires continuous cooling. However, the cost of operating the device under such conditions can be quite high. In an effort to improve the device's efficiency at higher temperatures and reduce the need for cooling, the ZnO window layer used in the previous study will be replaced with an SnO_2 layer. This replacement is expected to enable the device to maintain its optimal efficiency at higher temperatures, thereby improving the operating conditions and reducing the overall operating costs. The SnO_2 layer is expected to provide a better operating condition for the device by allowing it to maintain its optimal efficiency at higher temperatures. This is because the SnO_2 layer has better thermal stability than the ZnO layer used in the previous study. By replacing the ZnO layer with an SnO_2 layer, the device will be able to operate at higher temperatures without experiencing a significant reduction in its efficiency. This will, in turn, reduce the need for continuous cooling, thereby improving the overall operating conditions and reducing the operating costs [29], [30]. The study will focus on the effect of temperature on the cell efficiency parameters including V_{OC}, J_{SC}, *FF*%, η%, and *QE*%.

The remaining sections of this paper are structured as follows. In Section II, the numerical modeling approach is presented and details about the material parameters uti-

lized are provided. This section encompasses the methodology for device simulation and modeling, the input parameters employed, and the mathematical equations utilized. Section III comprises the results and discussion, organized with subheadings such as the impact of working temperature on device performance and the influence of deep defects in layers on solar cell performance. Lastly, the concluding remarks are presented in the final section of this paper.

II. Numerical Modeling and Material Parameters

The proposed design for a thin film solar cell involves using a glass substrate as a base, with a molybdenum layer deposited on top. On top of that, a 2500 nm thick layer of ZnTe (p-type) is suggested to be added, followed by a 20 nm thick layer of ZnSe (n-type) as a buffer layer, and a 200 nm thick layer of SnO_2 (n-type) as a replacement for ZnO. The effectiveness, the stability, and the ease of preparation of these materials have been taken into consideration. Fig. 1 shows how the layers are arranged.

The simulation has included calculations for a defect system at different temperatures, as well as a J-V characteristic analysis. The impact of temperature on the efficiency of the solar cell was also evaluated. In order to compare the performance of the defected and non-defected systems, a simulation has been conducted for a non-defected system at an optimum temperature. In this study, the SCAPS-1D simulation software has been employed to simulate the suggested device and calculate the results.

This software is capable of solving the fundamental semiconducting equations for electron-hole pairs, based on Poisson's Equations (4) and (5):

$$\frac{d^2\Psi}{dx^2} = \frac{e}{\epsilon_o \epsilon_r}[p(x) - n(x) + N_D - N_A + \rho_P - \rho_n] \quad (4)$$

where Ψ is the electrostatic potential, e is the electrical charge, ε_r is the relative permittivity, ε_o is the vacuum permittivity, p and n are the concentrations of holes and electrons, respectively, N_D is the charged impurities of donor, N_A is the charged impurities of acceptor, p_p is the distribution of holes, and p_n is the distribution of electrons.

The continuity equations for electrons and holes are also considered in the simulation:

$$\frac{dJ_n}{dx} = \frac{dJ_p}{dx} = G - R \quad (5)$$

where J_n represents the densities of electron current, J_p represents the densities of hole current, R is the rate of recombination, and G is the rate of generation.

In semiconductors, carrier transport is represented by the electron and hole current densities that are generated by drift and diffusion. The equation that follows can be used to express the electron current densities, J_n:

$$J_n = D_n \frac{dn}{dx} + \mu_n n \frac{d\varphi}{dx} \quad (6)$$

where D_n is the electron diffusion coefficient, n is the electron concentration, dn/dx is the gradient of the electron concentration, μ_n is the electron mobility, and $d\varphi/dx$ is the gradient of the electrostatic potential.

The hole current densities, J_p, can be expressed by using the following equation:

$$J_p = D_p \frac{dp}{dx} + \mu_p p \frac{d\varphi}{dx} \quad (7)$$

Tables I and II depict the necessary input parameters for the suggested thin-film solar cell device. These information boundaries have been chosen in view of the ideal qualities announced in the writing [31]-[33].

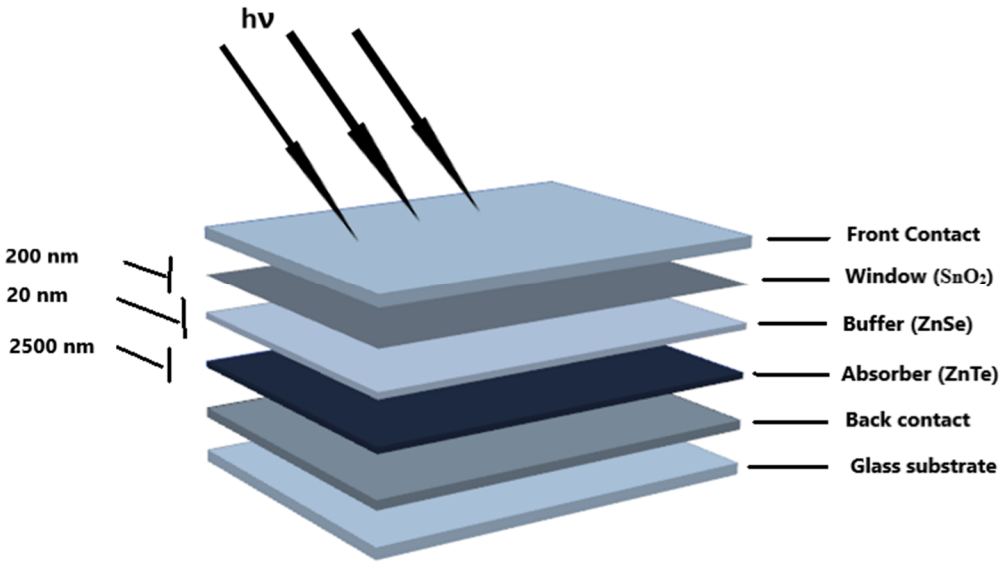

Fig. 1. Schematic structure of a thin film- based solar cell

TABLE I
THE INFORMATION BOUNDARIES UTILIZED FOR THE PROPOSED THIN-FILM SOLAR CELL DEVICE

Parameters	p -ZnTe	n- ZnSe	SnO_2
W (nm)	2.50	0.02	0. 20
E_g (eV)	2.26	2.90	3.60
χ (eV)	3.50	4.09	4.0
ε_r	9.67	10	9
N_C (cm^{-3})	7×10^{16}	1.5×10^{18}	2.2×10^{18}
N_V (cm^{-3})	2×10^{19}	1.8×10^{18}	1.8×10^{19}
$V_{e\text{-}th}$(cm/s)	1×10^{7}	1×10^{7}	1×10^{7}
$V_{p\text{-}th}$ (cm/s)	1×10^{7}	1×10^{7}	1×10^{7}
μ_e (cm^2/Vs)	330	50	100
μ_p (cm^2/Vs)	80	20	25
N_D (cm^{-3})	0	1×10^{17}	1×10^{18}
N_A (cm^{-3})	2×10^{15}	0	0

TABLE II
ELECTRICAL AND OPTICAL PROPERTIES OF BACK AND FRONT CONTACT USED IN SCAPS SIMULATION

Electrical Properties		Back contact	Front contact
Thermionic emission surface recombination velocity (cm/s)	Electron	1×10^{7}	1×10^{7}
	Holes	1×10^{7}	1×10^{7}
Metal work function (eV)		4.625	4.1
Majority carrier barrier height (eV)	Relative to E_F	0.4	0.1
	Relative to E_V or E_C	- 0.1227	0.0199
Allow contact tunneling	Effective mass of electron	1	1
	Effective mass of holes	1	1
Optical Properties	Filter Mod	Reflection	Transmission
	Filter value	0.8	0.95
	Complement of filter value	0.2	0.05

TABLE III
BULK DEFECTS PROPERTIES IN ZnTe/ZnSe/SnO2 DEVICE

Defect	ZnTe	ZnSe	SnO_2
Charge type	neutral	neutral	neutral
Total density (cm^{-3}): Uniform	2×10^{14}	1×10^{18}	1.0×10^{15}
Energy distribution: Gauss	E_t = 0.75 eV above EV E_{kar} = 0.1 eV	E_t = 1.2 eV above EV E_{kar} = 0.1 eV	Et = 1.8 eV above EV E_{kar} = 0.1 eV
Capture cross section area of electrons (cm^2)	1.0×10^{-13}	1.0×10^{-15}	1.0×10^{-15}
Capture cross section area of holes (cm^2)	1.0×10^{-15}	5.0×10^{-13}	5.0×10^{-13}

In polycrystalline thin-film ZnTe solar cells, deep electronic states often occur in high concentrations relative to the shallow acceptors. In some instances, these deep electronic states can be the dominant source of free carriers.

This pins the Fermi level and can distort the values obtained through Admittance spectroscopy measurements, including activation energy and apparent capture cross-section. In order to investigate the effect of defects, a defect has been assumed to be present in the absorber (ZnTe) layer, buffer (ZnSe) layer, and window (SnO_2) layer, as shown in Table III.

III. Results and Discussion

The reproduced J-V characterization at various temperatures at the damaged framework is displayed in Fig. 2.

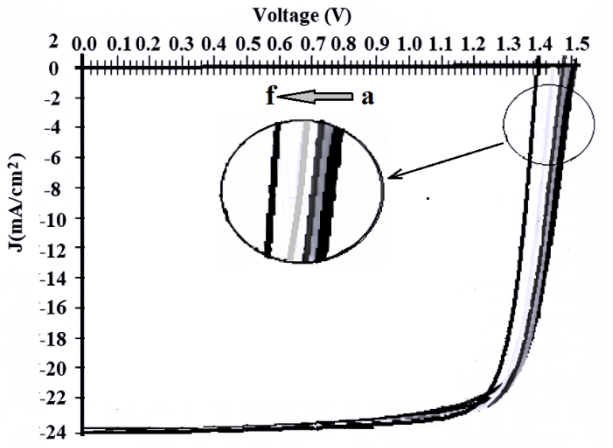

Fig. 2. Current mode with voltages: a) 300 K, b) 330 K. c) 360 K. d) 375 K. e) 420 K. f) 450 K

The effect of temperature on the cell efficiency parameters (V_{OC}, J_{SC}, FF%, and η%) is shown in Table IV, which displays the parameters of solar cell efficiency. It is demonstrated that the operating temperature had no significant effect on the J_{SC}, which only slightly increased to a steady limit. This is because the decrease in the band-hole energy that is calmly impacted [34]. Consequently, more photons within the radiation's reach will be capable of forming electron-hole pairs. On the other hand, as the temperature rises, V_{OC} decreases slightly. The temperature-dependent reverse saturation current (I_S) is to blame for the decrease in V_{OC} values with temperature [35]. One more fundamental component that makes sense of the decrease in V_{OC} with working temperature is the characteristic transporter focus, (n_i) [36], [37]. The absorber layer's bandgap typically has a narrow range. The electron-hole pair's recombination may be facilitated by the bandgap's narrowing. The temperature typically decreases bandgap stability [38], [39]. If the fact that an increase in the amplitude of the atomic vibrations is accompanied by an increase in the thermal energy is considered, this behavior can be better comprehended. The material's linear expansion coefficient is used to measure this effect. The material's electrons see less potential when there is more space between the atoms, which reduces the energy bandgap's size.

TABLE IV
SOLAR CELL OPERATING CHARACTERISTICS AT DIFFERENT OPERATIN TEMPERATURES

T (K)	V_{OC}(V)	J_{SC} (mA/cm^2)	FF%	η (%)
300	1.5057	24.262726	74.31	27.15
315	1.5010	24.276326	75.47	27.50
330	1.4966	24.289040	76.37	27.76
345	1.4921	24.300947	77.04	27.93
360	1.4875	24.312107	77.51	28.03
365	1.4858	24.315669	77.64	28.05
370	1.4840	24.319153	77.76	28.06
375	**1.4819**	**24.322560**	**77.88**	**28.07**
380	1.4798	24.325889	77.97	28.07
385	1.4771	24.329139	78.08	28.06
390	1.4738	24.332307	78.20	28.04
405	1.4607	24.341291	78.64	27.96
420	1.4400	24.349374	79.05	27.79
435	1.4212	24.356381	79.51	27.52
450	1.3939	24.362200	79.88	27.13

The *FF*% is somewhat expanded with temperature to a consistent state temperature limit. This temperature limit is 400 K. The effectiveness of slight thin-film structure solar cells increments with temperatures up to 375 K. At a temperature higher than 375 K, the proficiency has been tumbling down. At higher temperatures, boundaries like the electron and opening motilities, transporter focuses, and bandgaps of the materials would be impacted which brings about lower proficiency of the phones [40]. In conclusion, the optimal temperature will be chosen here as 375 K.

One of the most crucial parameters that affect the performance of the solar cells and the current transport across the heterojunction is the band alignment. The band outline of solar-cell construction can be obtained by utilizing the SCAPS-1D programming program. Figs. 3 depict the model (0 - 2.5 μm is the ZnTe layer, 2.5 - 2.52 μm is the ZnSe layer, and 2.52 - 2.72 μm is the SnO2 layer) band diagram.

The band diagram is an important tool to understand the energy levels and carrier transport mechanisms in a solar cell device. In this specific case, the band diagram shows that the conduction band offset between the ZnTe absorber and ZnSe buffer layers is approximately 0.38 eV, which is close to the maximum band offset requirement of 0.4 eV for achieving high efficiency as reported earlier [41]. The band diagram also highlights four recombination regions, which are: (1) the recombination at the ZnTe layer back contact, (2) the bulk recombination in the ZnTe absorber layer, (3) the space charge depletion layer in ZnTe, and (4) the absorber/buffer interface recombination. By using a thin absorber layer, the distance of the bulk recombination region in the ZnTe absorber layer (R2) is reduced, and the back contact is kept very close to the depletion region (R3). This results in a noticeable increase in the recombination of the back contact, where a large amount of photogenerated carriers is recombined, leading to a decrease in the overall efficiency of the solar cell device. Moreover, the bandgap energy of each layer (i.e., absorber, buffer, and window layers) depends on temperature, as listed in Table V. The effect of increased temperature on the depletion region between the absorber layer and buffer layer is shown in Figs. 3(a), (b), and (c). This effect can contribute to the total loss that occurs within and outside the active region, leading to an increase in the short current density (J_{SC}) and a decrease in the quantum efficiency (η). The losses are mainly due to the Non-Radiative Auger recombination of the injected carriers, internal losses due to defects in the active region and the surfaces of contact between the layers, and losses due to the effect of temperature on the refractive index in the semiconductor, which results in a change in the optical inventory factor as reported earlier [42], [43].

It appears that the quantum productivity profiles at various temperature values show that the solar cell has a peak reaction to enlightenment frequency in the scope of 520–800 nm with a *QE*% going from 80–90% and begins to diminish under 520 nm because of recombination and retention in the safeguard and cushion layers.

TABLE V
BANDGAP ENERGY DEPENDS ON TEMPERATURE

	Bandgap energy (eV)		
T (K)	Absorber (ZnTe)	Buffer (ZnSe)	Window (ZnO)
300	2.26	2.90	3.60
375	2.34	2.98	3.68
450	2.42	3.06	3.76

An absorption edge at approximately 800 nm may be attributed to doping-induced vacancy levels in the energy gap, and the absorption maxima at around 530 nm are consistent with the input ZnTe value. It is also noted that the temperatures in the 300–450 K range had no discernible effect on quantum efficiency, possibly due to the short time period studied and the absence of shallow-level defects near the band edge.

The majority of manufactured thin-film solar cells have flaws that reduce their efficiency because it is difficult to make a perfect semiconductor solar cell thin-film crystal.

Defects open up new recombination routes, allowing electron-hole recombination to turn the generated light into heat rather than electricity. The solar cell's carrier lifetime and quantum efficiency are both reduced as a result of these defects, which also result in deep energy levels in the semiconductor bandgap. Because recombination centers prevent carriers from reaching the terminals of solar cells, they are ineffective. A simulation has been carried out at the ideal temperature of 375 K without any flaws in order to evaluate the performance of an ideal thin-film solar cell. Fig. 5 shows the J-V characteristics of both defect and ideal crystals at this temperature, and Table VI summarizes the parameters of efficiency. The ideal and defect systems have comparable V_{oc} values, yet the defect displays lower efficiency because of recombination and limited energy levels caused by the imperfections.

Fig. 6(a) displays the band diagram for the defected system, while Fig. 6(b) shows the non-defect system.

These diagrams offer valuable insights into the effects of defects on band structure and band alignment, thus expanding the scope for modifying the band structure of 2D materials through defect engineering. In particular, the pristine center region of the defected system features a Fermi level located roughly mid-gap, approximately 0.75 eV above the valence band for ZnTe, 1.2 eV above the valence band for ZnSe, and 1.8 eV above the valence band for SnO_2. Furthermore, the impact of defects on quantum efficiency has been investigated for the thin-film solar cell.

Fig. 7 displays the *QE*% profiles for both the defective and non-defective crystals.

The quantum efficiency has been measured in the wavelength range of 300-800 nm, and the results show that the *QE*% value of the defected system is lower than that of the perfect crystal system in the range of 300-520 nm.

This reduction in the quantum efficiency of the defected system results in a decrease in the overall efficiency of the solar cell device, as demonstrated in Fig. 5 and Table VI. Therefore, it is important for manufacturing processes to strive to prepare near-perfect crystal semiconductor layers with minimal defects to enhance and increase solar cell efficiency.

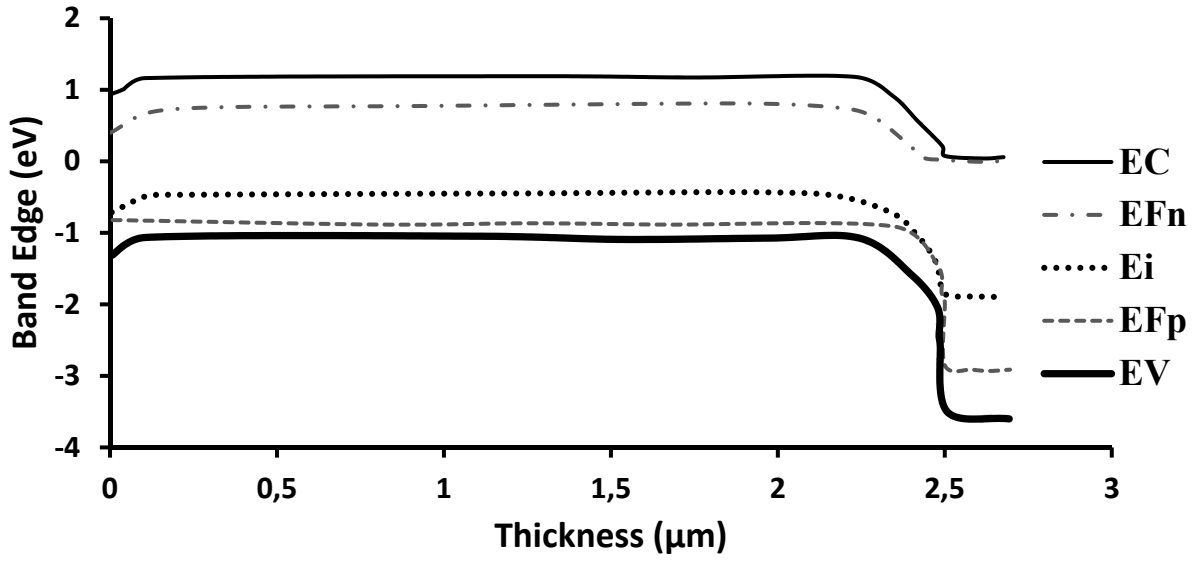

(a) 300 K

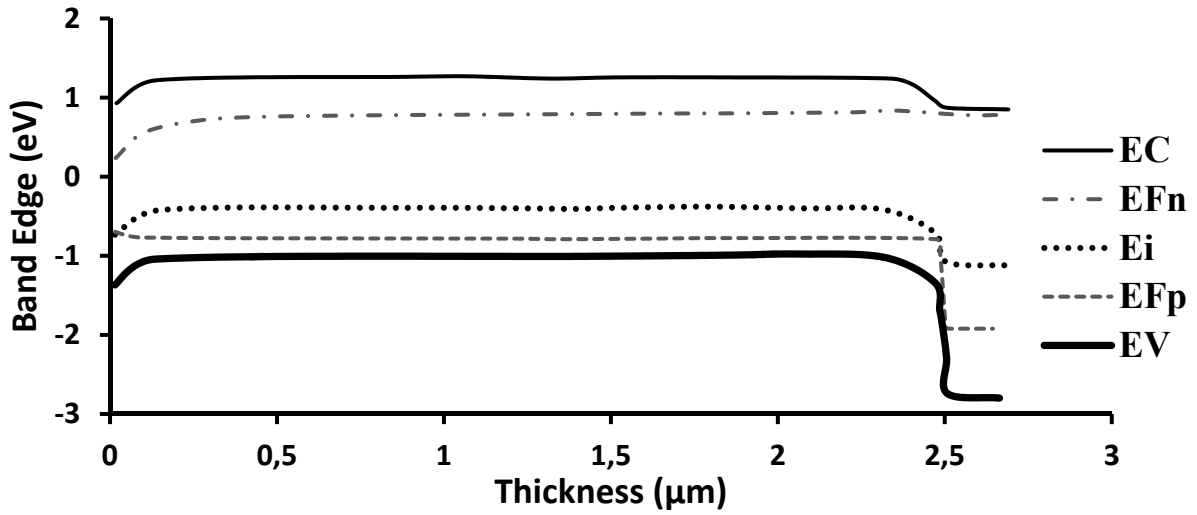

(b) 375 K

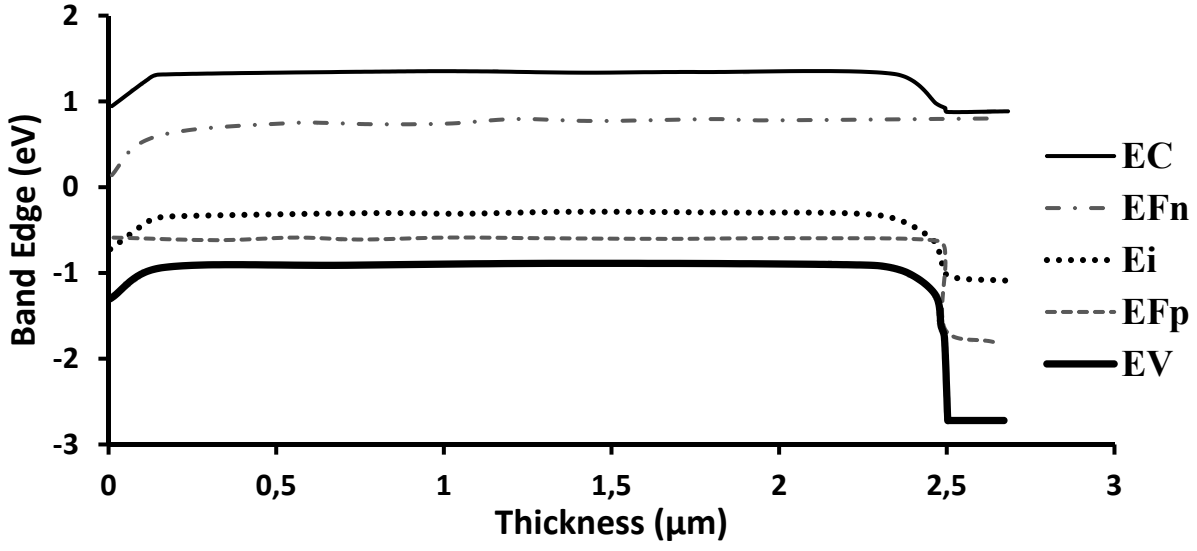

(c) 450 K

Figs. 3. Band diagram for thin film structure solar cells at different temperature degrees, 300, 375, and 450 K

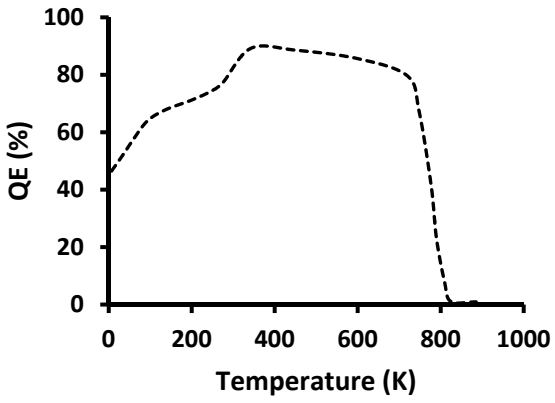

Fig. 4. Quantum efficiency of thin film solar cell at various operating temperature

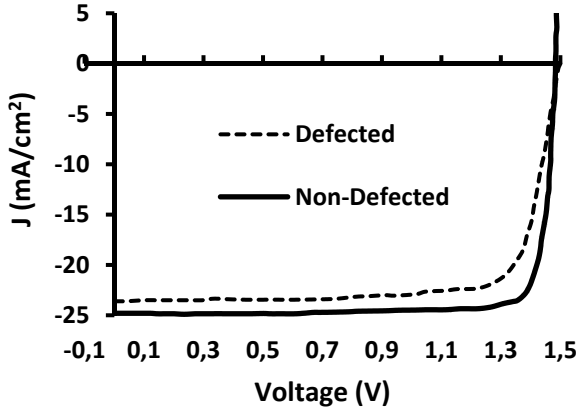

Fig. 5. Current mode with voltage, at the optimum temperature (T = 300 K)

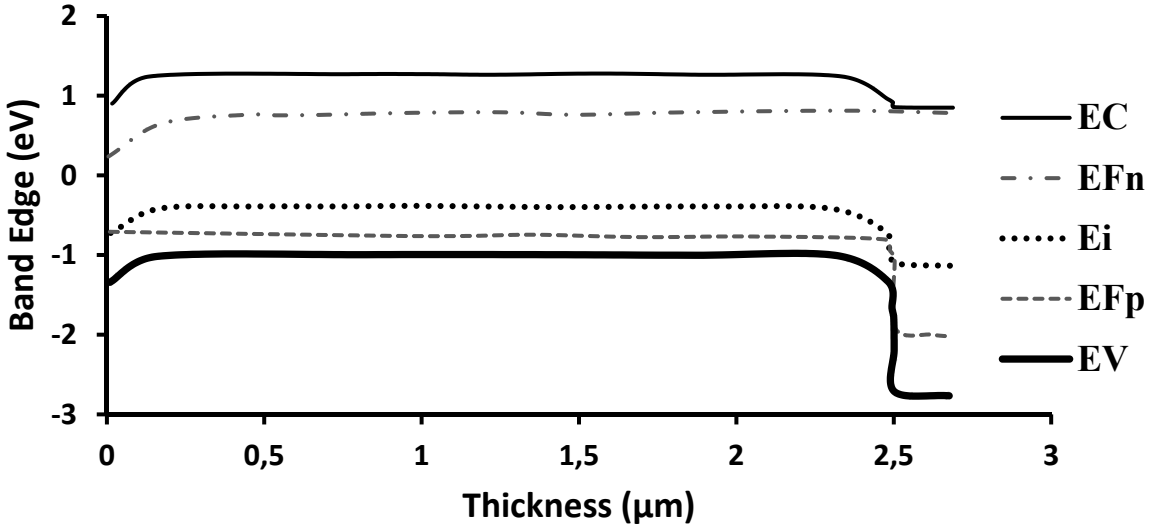

(a) Defected System

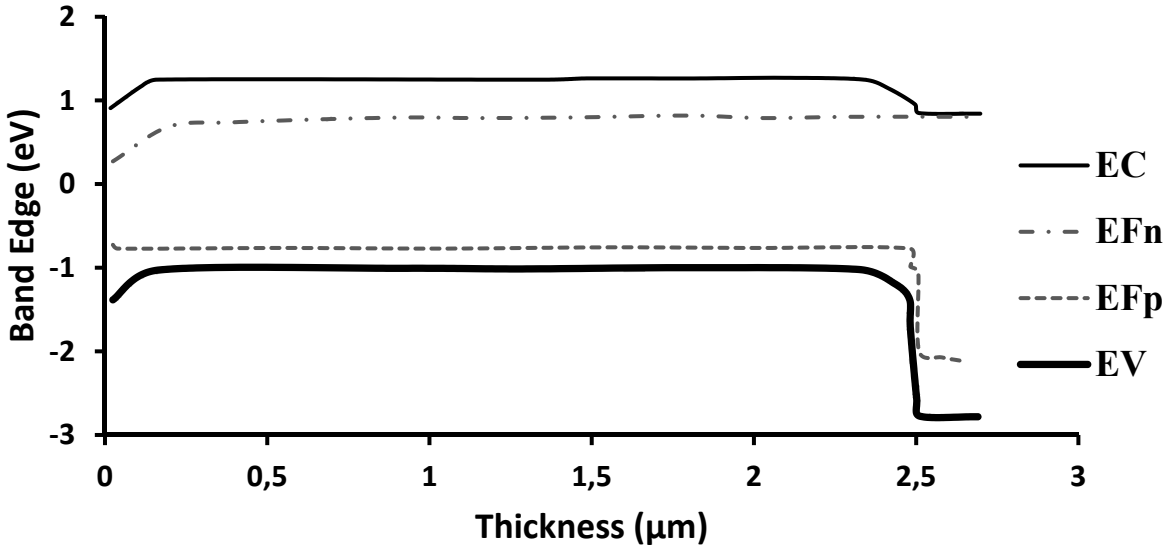

(b) Non-Defected system

Figs. 6. Band Diagram, (a) with defect, (b) without defect , at the optimum temreature (T = 300 K)

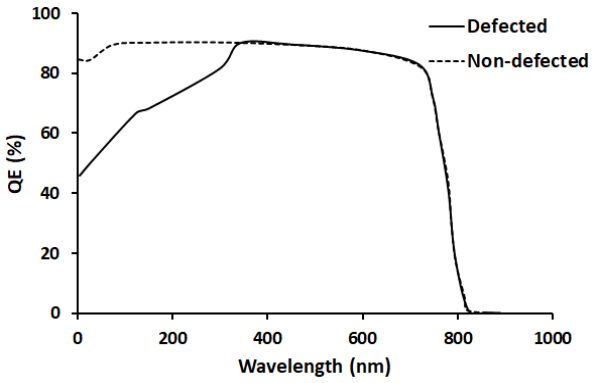

Fig. 7. Quantum efficiency of thin film solar cell at various operating temperature(red) with defect. (blue) without defect, at the optimum temperature (T = 300 K)

TABLE VI
DEFECT DEPENDENCY

	V_{OC}(V)	J_{SC}(mA/cm^2)	FF%	η (%)
With Defect	1.4819	24.322560	77.88	28.07
Without Defect	1.4641	25.469234	85.68	31.95

IV. Conclusion

Mo/ZnTe/ZnSe/SnO_2 thin-film solar cells have been optimized thanks to the simulation results obtained by using the SCAPS-1D software. According to the results, using SnO_2 as a window layer instead of ZnO has a number of benefits. First off, it permits a higher operating temperature of 375 K, which is ideal for the performance of the solar cell, whereas the ideal operating temperature for ZnO has been discovered to be 300 K. The steady-state values for V_{OC}, J_{SC}, and *FF* percent, along with the elevated bandgap energy, demonstrate that the solar cell can achieve improved efficiency at this higher temperature. In addition, unlike the earlier use of ZnO, the use of SnO_2 does not require constant cooling. This feature improves the thin-film solar cell's usability and affordability, making it a promising contender for solar photovoltaic applications. In order to prevent cell efficiency from being hampered and lower quantum efficiency from occurring, it is imperative to address crystal structure flaws.

Future work should concentrate on reducing manufacturing flaws to maximize the efficiency of these solar cells. The performance and effectiveness of the Mo/ZnTe/ZnSe/SnO_2 thin-film solar cells can be further improved by making sure that strict quality control procedures are followed, which will help to develop high-efficiency, affordable, and environmentally friendly solar energy technologies.

Acknowledgements

We might want to offer our true thanks to Dr. Marc Burgelman from the College of Gent, Belgium, for liberally furnishing us with the SCAPS-1D reenactment programming. We also want to express our sincere gratitude to Ajman University for supporting this study.

References

[1] M. Akhsassi, et al., Experimental investigation and modeling of the thermal behavior of a solar PV module. *Solar Energy Materials and Solar Cells,* Vol. 180: 271-279, 2018.

[2] Delfianti, R., Nusyura, F., Priyadi, A., Abadi, I., Soeprijanto, A., Optimizing the Price of Electrical Energy Transactions on the Microgrid System Using the Shortest Path Solution, (2022) *International Review on Modelling and Simulations (IREMOS)*, 15 (4), pp. 279-286. doi:https://doi.org/10.15866/iremos.v15i4.22712

[3] Covill, D., et al., Parametric finite element analysis of steel bicycle frames: the influence of tube selection on frame stiffness. *Procedia Engineering,* Vol. 112: 34-39, 2015.

[4] U. Kingsley, P.E. Imoisili, and D. Adgidzi, Finite element analysis of bamboo bicycle frame. *British Journal of Mathematics & Computer Science,* Vol. 5(5): 583, 2015.

[5] Hassouna, F., Tubaileh, M., Road Traffic Casualties in West Bank: Trends Analysis and Modeling, (2021) *International Review of Civil Engineering (IRECE)*, 12 (2), pp. 101-107. doi:https://doi.org/10.15866/irece.v12i2.19907

[6] P.C. Marchal, J.G. Ortega, and J.G. García, Production Planning, Modeling and Control of Food Industry Processes. *Springer Nature,* 2019.

[7] Al-Shawesh, Y., Lim, S., Nujaim, M., Analysis of the Design Calculations for Electrical Earthing Systems, (2021) *International Review of Electrical Engineering (IREE)*, 16 (2), pp. 104-117. doi:https://doi.org/10.15866/iree.v16i2.16839

[8] H. Biemans, et al., Future water resources for food production in five South Asian river basins and potential for adaptation—A modeling study. *Science of the Total Environment,* Vol. 468: S117-S131, 2013.

[9] Espinel, E., Rojas, J., Florez, E., 2D Simulation of Two-Phase Flow for Water Jet Cutting Processes with OpenFOAM®, (2021) *International Review on Modelling and Simulations (IREMOS)*, 14 (4), pp. 301-310. doi:https://doi.org/10.15866/iremos.v14i4.19332

[10] Orjuela Abril, S., Acevedo, C., Cardenas Gutierrez, J., Computational Fluid Dynamics Analysis of Combined Cycle Power Plant Heat Exchanger with OpenFOAM® Software, (2020) *International Review on Modelling and Simulations (IREMOS)*, 13 (5), pp. 319-328. doi:https://doi.org/10.15866/iremos.v13i5.18891

[11] Romero Garcia, G., Florez Solano, E., Cardenas, J., Experimental and CFD Characterization of the Jacket Vessel Heat Transfer Process, (2020) *International Review on Modelling and Simulations (IREMOS)*, 13 (5), pp. 329-336. doi:https://doi.org/10.15866/iremos.v13i5.18882

[12] R. Younas, et al., Computational modeling of polycrystalline silicon on oxide passivating contact for silicon solar cells. *IEEE Transactions on Electron Devices,* Vol. 66(4): 1819-1826, 2019.

[13] Qasim, M., Velkin, V., Maximum Power Point Tracking Techniques for Micro-Grid Hybrid Wind and Solar Energy Systems - a Review, (2020) *International Journal on Energy Conversion (IRECON)*, 8 (6), pp. 223-234. doi:https://doi.org/10.15866/irecon.v8i6.19502

[14] Zizoui, M., Tabbache, B., Zia, M., Benbouzid, M., Control of Isolated Photovoltaic-Battery-Ultracapacitor Microgrid for Remote Areas, (2020) *International Journal on Energy Conversion (IRECON)*, 8 (2), pp. 38-44. doi:https://doi.org/10.15866/irecon.v8i2.18969

[15] A. Verma, and P. Asthana, Modeling of Thin Film Solar Photovoltaic Based on Zno/Sns Oxide-Absorber Substrate Configuration. *Int. Journal of Engineering Research and Applications,* Vol. 4(6):12-18, 2014.

[16] Tyagi, A., et al., An analytical model for the electrical characteristics of passivated carrier-selective contact (CSC) solar cell. *IEEE Transactions on Electron Devices,* Vol. 66(3): 1377-1385, 2019.

[17] N. Amin, K. Sopian, and M. Konagai, Numerical modeling of CdS/CdTe and CdS/CdTe/ZnTe solar cells as a function of CdTe thickness. *Solar energy materials and solar cells,* Vol. 91(13): 1202-1208, 2007.

[18] O. Skhouni, et al., Numerical study of the influence of ZnTe thickness on CdS/ZnTe solar cell performance. *The European Physical Journal Applied Physics,* Vol. 74(2): p. 24602, 2016.
[19] P. Chelvanathan, M.I. Hossain, and N. Amin, Performance analysis of copper–indium–gallium–diselenide (CIGS) solar cells with various buffer layers by SCAPS. *Current Applied Physics,* Vol. 10(3): S387-S391, 2010.
[20] Wagner, S., et al., CuInSe2/CdS heterojunction photovoltaic detectors. *Applied Physics Letters,* 1974. Vol. 25(8): 434-435, 1974.
[21] Singh, P., et al., Temperature dependence of I–V characteristics and performance parameters of silicon solar cell. *Solar Energy Materials and Solar Cells,* Vol. 92(12): 1611-1616, 2008.
[22] S.H. Zyoud, et al., Numerical modeling of high conversion efficiency FTO/ZnO/CdS/CZTS/MO thin film-based solar cells: Using SCAPS-1D software. *Crystals,* Vol. 11(12): p. 1468, 2021.
[23] S.H. Zyoud, et al., Numerical modelling analysis for carrier concentration level optimization of CdTe heterojunction thin film–based solar cell with different non–toxic metal chalcogenide buffer layers replacements: using SCAPS–1D software. *Crystals,* Vol. 11(12): p. 1454, 2021.
[24] Zyoud, S., Zyoud, A., Effect of Absorber (Acceptor) and Buffer (Donor) Layers Thickness on Mo/CdTe/CdS/ITO Thin Film Solar Cell Performance: SCAPS-1D Simulation Aspect, (2021) *International Review on Modelling and Simulations (IREMOS)*, 14 (1), pp. 10-17. doi:https://doi.org/10.15866/iremos.v14i1.19953
[25] Zyoud, S., Zyoud, A., Abdelkader, A., Ahmed, N., Numerical Simulation for Optimization of ZnTe-Based Thin-Film Heterojunction Solar Cells with Different Metal Chalcogenide Buffer Layers Replacements: SCAPS-1D Simulation Program, (2021) *International Review on Modelling and Simulations (IREMOS)*, 14 (2), pp. 79-88. doi:https://doi.org/10.15866/iremos.v14i2.19954
[26] M. Burgelman, et al., Modeling thin-film PV devices. Progress in Photovoltaics: *Research and Applications,* Vol. 12(2-3): 143-153, 2004.
[27] K. Decock, S. Khelifi, and M. Burgelman, Modelling multivalent defects in thin film solar cells. *Thin Solid Films,* Vol. 519(21): 7481-7484, 2011.
[28] J. Verschraegen, and M. Burgelman, Numerical modeling of intra-band tunneling for heterojunction solar cells in SCAPS. *Thin Solid Films,* Vol. 515(15): 6276-6279, 2007.
[29] S. Yu, et al., Organic thin-film transistors with polymeric gate insulators. *Journal of non-crystalline solids,* Vol. 354(14): 1516-1521, 2008.
[30] J.K. Saha, et al., Significant improvement of spray pyrolyzed ZnO thin film by precursor optimization for high mobility thin film transistors. *Scientific reports,* Vol. 10(1): 1-11, 2020.
[31] N. Amin, et al., Prospects of back surface field effect in ultra-thin high-efficiency CdS/CdTe solar cells from numerical modeling. *International journal of photoenergy,* Vol. 2010: 1-8, 2010.
[32] T. Aramoto, et al., 16.0% efficient thin-film CdS/CdTe solar cells. *Japanese Journal of Applied Physics,* Vol. 36(10R): 6304, 1997.
[33] S. Hossain, et al., A Numerical Study on the Prospects of High Efficiency Ultra Thin Zn x Cd (1-x) S/CdTe Solar Cell. *Chalcogenide letters,* Vol. 8(4): 263-272, 2011.
[34] P. Singh, and N.M. Ravindra, Temperature dependence of solar cell performance—an analysis. *Solar energy materials and solar cells,* Vol. 101: 36-45, 2012.
[35] A.A.A. Al-Khazzar, Behavior of four Solar PV modules with temperature variation. *Int. J. Renew. Energy Res,* Vol. 6(3): 1091-1099, 2016.
[36] A. Sproul, and M. Green, Improved value for the silicon intrinsic carrier concentration from 275 to 375 K. *Journal of applied physics*, Vol. 70(2): 846-854, 1991.
[37] A. Sproul, and M. Green, Intrinsic carrier concentration and minority-carrier mobility of silicon from 77 to 300 K. *Journal of Applied Physics,* Vol. 73(3): 1214-1225, 1993.
[38] J.-W. Gong, et al., Temperature feedback control for improving the stability of a semiconductor-metal-oxide (SMO) gas sensor. *IEEE Sensors Journal,* Vol. 6(1): 139-145, 2006.
[39] K. O'donnell, and X. Chen, Temperature dependence of semiconductor band gaps. *Applied physics letters,* Vol. 58(25): 2924-2926, 1991.
[40] T. Nakada, and M. Mizutani, 18% efficiency Cd-free Cu (In, Ga) Se2 thin-film solar cells fabricated using chemical bath deposition (CBD)-ZnS buffer layers. *Japanese Journal of Applied Physics,* Vol. 41(2B): L165-L167, 2002.
[41] R. Shikler, et al., Measuring minority-carrier diffusion length using a Kelvin probe force microscope. *Physical Review B,* Vol. 61(16): 11041-11046, 2000.
[42] Wang, L., et al., A review on experimental measurements for understanding efficiency droop in InGaN-based light-emitting diodes. *Materials,* Vol. 10(11): 1233, 2017.
[43] S.H. Zyoud, A. Abdelkader, and A.H. Zyoud, The Impact of Temperature on the Performance of Semiconductor Laser Diode. *Int. J. Adv. Sci. Technol,* Vol. 29: 1167-1180, 2020.

Authors' information

[1]Department of Mathematics and Sciences, Ajman University, Ajman, United Arab Emirates.

[2]Nonlinear Dynamics Research Center (NDRC), Ajman University, Ajman, United Arab Emirates.

[3]Department of Chemistry, An-Najah National University, Nablus, Palestine.

Samer H. Zyoud was born and raised in Palestine, where he is originally from. He continued his education and graduated with a B.Sc. in physics degree from Mosul University, Iraq, in 2001. Afterward, he got an M.Sc. degree in 2003 with a degree in physics from the University of Baghdad in Baghdad, Iraq. Samer works as a senior lecturer at Ajman University in Ajman, United Arab Emirates, at the moment. He is pursuing a Ph.D. simultaneously at the University of Sains Malaysia in Penang, Malaysia. Solar cells, photocatalysts, sensors, and semiconductor lasers are just a few of the areas in which he studies nanostructures on thin films in his work.
E-mail: s.zyoud@ajman.ac.ae

Ahed H. Zyoud (corresponding author) was born in Seilat Al-Harthiya, Palestine, in 1973. In 1996, he obtained his B.Sc. degree from Yarmouk University in Jordan. Later, in 2000, he earned his M.Sc. degree from An-Najah National University in Palestine. In 2009, he successfully completed his Ph.D. at the same university. Currently, Zyoud holds the position of professor at the Chemistry Department of An-Najah National University in Palestine. His primary research focus revolves around nanotechnology and materials, specifically their preparation and characterization. Additionally, he explores the applications of these nanomaterials, particularly in the fields of thin film photovoltaic technology and the degradation of organic pollutants in water.
E-mail: ahedzyoud@najah.edu